

Modeling Emission from the Supermassive Black Hole in the Galactic Center with GRMHD Simulations

Kyle W. Martin,¹ Siming Liu,² Chris Fragile,³ Cong Yu,⁴ and Chris L. Fryer^{2,5}

ABSTRACT

Sagittarius (Sgr) A* is a compact radio source at the Galactic center, powered by accretion of fully ionized plasmas into a supermassive black hole of $\sim (3 - 4) \times 10^6 M_{\odot}$. However, the radio emission cannot be produced through the thermal synchrotron process by a gravitationally bounded flow (Liu & Melia 2001). General relativistic magneto-hydrodynamical (GRMHD) simulations of black hole accretion show that there are strong unbounded outflows along the accretion. With the flow structure around the black hole given by GRMHD simulations, we investigate whether thermal synchrotron emission from these outflows may account for the observed radio emission and discuss the implications of this study on these GRMHD simulations and possible production of non-thermal particles by this source. We find that simulations producing relatively high values of plasma β cannot produce the radio flux level without exceeding the X-ray upper limit set by *Chandra* observations through the bremsstrahlung process. The predicted radio spectrum is also harder than the observed spectrum both for the one temperature thermal model and a simple nonthermal model with a single power-law electron distribution. Since higher frequency emission is produced at smaller radii, the electron temperature needs to be lower than the gas temperature near the black hole to reproduce the observed radio spectrum. A more complete modeling of the radiation processes, including the general relativistic effects and transfer of polarized radiation, will give more quantitative constraints on physical processes in Sgr A* with the current multi-wavelength, multi-epoch, and polarimetric observations of this source.

¹Physics Department, University of New Mexico, Albuquerque, NM 87131; kmartin1@unm.edu

²Los Alamos National Laboratory, Los Alamos, NM 87545; liusm@lanl.gov

³Physics & Astronomy, College of Charleston, Charleston, SC 29424; fragilep@cofc.edu

⁴National Astronomical Observatories/Yunnan Observatory, Chinese Academy of Science, Kunming, Yunnan 650011, China; yccit@yahoo.com.cn

⁵Physics Department, The University of Arizona, Tucson, AZ 85721; fryer@lanl.gov

Subject headings: acceleration of particles — black hole physics — Galaxy: center
— plasmas — radiation mechanisms: thermal, non-thermal

1. Introduction

Sagittarius (Sgr) A*, the compact radio source at the Galactic center, is powered by accretion of a supermassive black hole of $\sim (3 - 4) \times 10^6 M_{\odot}$ (Schödel et al. 2002; Ghez et al. 2004) in the prevailing stellar winds in the Galactic center region (Melia 1992). The bolometric luminosity of Sgr A* is more than 9 orders of magnitude lower than the corresponding Eddington luminosity, suggesting a radiatively inefficient accretion flow (Melia et al. 2001; Yuan et al. 2003). The radiative cooling processes therefore may be ignored while studying the dynamics of the accretion flow near the black hole, which simplifies the dynamical equations and the corresponding numerical algorithms significantly. Several general relativistic magneto-hydrodynamical (GRMHD) codes have been developed over the past few years to study the structure of non-radiative accretion flows near black holes quantitatively (De Villiers et al. 2003; Gammie et al. 2003; Anninos et al. 2005). Given the extensive observations available for this supermassive black hole, it provides perhaps the best opportunity to study the physical processes in the strong gravity near black holes with GRMHD simulations (Falcke et al. 2000; Huang et al. 2008).

The observed linear polarization and variability of the millimeter to near-infrared (NIR) emissions suggest that they are produced by the synchrotron process near the black hole (Aitken et al. 2000; Melia et al. 2000; Genzel et al. 2003; Eckart et al. 2004, 2006). The longer wavelength emissions are circularly polarized (Bower et al. 2001) with weak linear polarization observed during frequent outbursts or flares (Zhao et al. 2004; Yusef-Zadeh et al. 2007), which in combination with the continuity of the centimeter to sub-millimeter spectrum suggests a synchrotron origin for the longer wavelength emissions as well (Falcke et al. 1998; An et al. 2005). The analogy of Sgr A* with radio loud AGNs also favors a synchrotron scenario for the radio emission. However, the longer wavelength flux densities are less variable than the millimeter and sub-millimeter flux densities, indicating emissions from relatively larger radii (Falcke & Markoff 2000; Liu & Melia 2001; Herrnstein et al. 2004). Indeed, the millimeter and higher frequency emissions have been explained reasonably well with an accretion torus within $\sim 10 r_S$ of the black hole, where r_S is the Schwarzschild radius (Melia et al. 2000; Goldston et al. 2005; Liu et al. 2007; Noble et al. 2007); And high spatial resolution VLBI observations do show that the intrinsic size of the millimeter emission region is within $20 r_S$ in radius (Bower et al. 2004; Shen et al. 2005). While

the general relativistic (GR) effects are important for these shorter wavelength emissions originating near the black hole (Falcke et al. 2000; Bromley et al. 2001), the longer wavelength emissions are produced beyond $\sim 10 r_S$ so that the GR effects are insignificant and one may readily use the GRMHD simulations to model the observed emission without using the sophisticated GR ray-tracing radiation transfer codes for the polarized synchrotron emission (Broderick & Loeb 2005; Huang et al. 2008).

High resolution X-ray observations with the *Chandra* space telescope shows that the quiescent X-ray excess from the direction of Sgr A* is extended and has ion emission lines in the spectrum, suggesting that the emission is mostly produced at large radii near the capture radius of the accretion flow by a plasma of a few keV in temperature (Baganoff et al. 2001, 2003; Xu et al. 2006). X-ray flares are routinely observed from the direction of Sgr A* (Belanger et al. 2006). Their spectra can be fitted with a featureless power law (Porquet et al. 2003), and they appear to be always accompanied by NIR flares, which are produced near the black hole (Eckart et al. 2004, 2006; Yusef-Zadeh et al. 2006, 2008). The correlation between the NIR and X-ray flares indicates a synchrotron self-Comptonization (SSC) origin for the X-ray flares (Markoff et al. 2001; Liu & Melia 2001), though the X-ray flares may also be produced via the bremsstrahlung process enhanced by instabilities related to the accretion process (Liu & Melia 2002; Tagger & Melia 2006). Recent observations of flares seem to favor a synchrotron process (Liu & Melia 2001; Dodds-Eden et al. 2009).

The quiescent state X-ray emission from the inner accretion flow therefore must be lower than the observed flux level. X-ray emission can be produced through both the SSC and bremsstrahlung processes. The observed high radio flux level and low upper limit of X-ray flux suggest that the radio emission cannot be produced via thermal synchrotron emission in a bounded flow (Liu & Melia 2001). It therefore has to be produced by unbounded outflows and/or by nonthermal populations of relativistic electrons. Given the non-radiative nature of the GRMHD simulations, strong outflows and winds appear to be inevitable, especially for highly spinning black holes (Noble et al. 2006; Hawley et al. 2007). In this paper, we investigate whether emissions from these simulated accretion flows can count for observations of Sgr A*, especially the low frequency radio emissions, self-consistently.

We carried out 2-dimensional (2D) GRMHD simulations with the Cosmos++ and HARM codes (Gammie et al. 2003; Anninos et al. 2005) assuming axis-symmetry of the accretion flow. The accretion disk therefore must be aligned with the equatorial planes of spinning black holes. The length scale is determined by the black hole mass. Since no radiative cooling is included, the density is scaled linearly with the mass accretion rate, and the gas temperature and plasma β , defined as the ratio of the gas pressure to the magnetic field pressure, are independent of the black hole mass and accretion rate. GRMHD

simulations give the gas density, pressure, and magnetic field. The gas temperature can be derived from the equation of state. The mass of the supermassive black hole in Sgr A* is well-measured by observations of stellar orbits around the black hole (Schödel et al. 2002; Ghez et al. 2004). One therefore needs to adjust the accretion rate, black hole spin, and electron distribution to fit the observed spectrum of Sgr A*. We consider both a one temperature and a two-temperature model of electrons in the thermal synchrotron emission scenario. For non-thermal synchrotron models, the electron distribution is assumed to follow a steep power-law with a low energy cutoff. In § 2 we discuss the methods that we used to model the emission spectra from the simulated accretion flows. A detailed discussion of our results and the implications are given in § 3.

2. Modeling the Emission Spectrum

We run the Cosmos++ code over a simulation domain of $218 r_S$ in radius. Initially, there is an equilibrium torus with the pressure maximum at $100 r_S$. Under the influence of the strong gravity of the central black hole, the torus evolves and the magneto-rotational-instability sets in and induces the accretion process (Balbus & Hawley 1991). Specific attributes of the accretion disc were examined and the magnetic field, gas temperature, and particle density profiles are shown in Figure 1. Because the simulation was run up to the dynamical time near $100 r_S$, the initial torus structure has not relaxed completely and, beside the cusped accretion torus in the inner region, which corresponds to the particle concentration within $100 r_S$, there is another high density region at $\sim 100 r_S$, which maps to the initial torus. If the simulation were allowed to run longer, this region of high density would be pulled closer to the black hole and merge with the inner accretion torus. The simulation also produces extremely high temperature regions along the polar directions, the polar regions within a half open angle of 6° and the inner $10 r_S$ region are excluded in our modeling of the emission for this simulation.

We first consider the simplest case, where electrons and ions reach thermal equilibrium throughout the simulation domain, so that the electron temperature is given by the gas temperature. The synchrotron emission coefficient at frequency ν is given by (Pacholczyk 1970; Mahadevan et al. 1996; Liu et al. 2006)

$$\mathcal{E}_\nu(\nu) = \frac{\sqrt{3}e^3}{4\pi m_e c^2} B n x_m I(x_m), \quad (1)$$

where

$$x_m = \frac{\nu}{\nu_c} \equiv \frac{4\pi m_e c \nu}{3eB\gamma_c^2}, \quad (2)$$

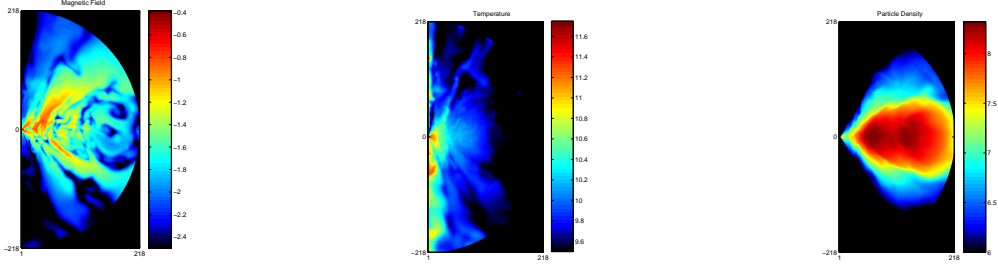


Fig. 1.— *Left:* The magnetic field in units of Gauss in a logarithmic color scale for the simulation with the Cosmos++. *Middle:* Same as the left panel but for the temperature in Kelvin. *Right:* Same as the left panel but for the particle number density in cm^{-3} . The outermost high density region corresponds to the position of the initial torus. If the simulation were to run longer this region of high density at about $100 r_S$ would merge with the inner high density region.

$$I(x_m) = 4.0505x_m^{-1/6}(1 + 0.40x_m^{-1/4} + 0.5316x_m^{-1/2}) \times \exp(-1.8899x_m^{1/3}), \quad (3)$$

$$\gamma_c = \frac{k_B T_e}{m_e c^2}, \quad (4)$$

where $T_e = T = P_{gas}m_p/2\rho k_B$ is the electron temperature and T , P_{gas} , ρ , B , n , e , m_e , c , and k_B indicate the gas temperature, pressure, mass density, magnetic field, particle density, the elementary charge unit, electron mass, speed of light, and the Boltzmann constant, respectively. The left and middle panels of Figure 2 show the profiles of \mathcal{E} at 1.0 and 100 GHz, respectively. The corresponding absorption coefficient κ_ν and the opacity τ along the light of sight of the accretion disk is given, respectively, by

$$\kappa_\nu = \frac{\mathcal{E}_\nu}{2\gamma_c m_e \nu^2}, \quad \tau = \int \kappa_\nu dl, \quad (5)$$

where the integration of τ is along the light of sight from the observer into the source region.

Then the observed flux density from the accretion flow (Melia et al. 2001)

$$F_\nu(\nu) = \frac{1}{D^2} \int I_\nu ds, \quad (6)$$

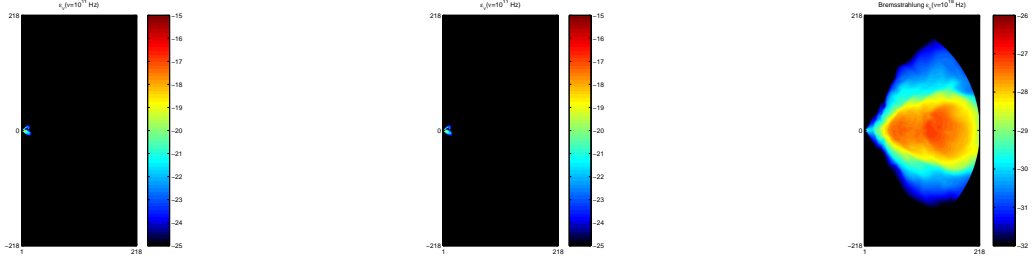


Fig. 2.— *Left:* The synchrotron emission coefficient in the plasma co-moving frame at 1.0 GHz in the c.g.s. units. *Middle:* Same as the left panel at 100 GHz. *Right:* The bremsstrahlung emission coefficient at 10^{18} Hz, which corresponds to ~ 4.1 keV in energy.

where

$$I_\nu = \int \mathcal{E}_\nu \exp(-\tau) dl,$$

is the specific intensity and D is the distance to the Galactic Center and the integration of F_ν is over the projected area of the source. For a face-on disk with the observer located at $z = D$, the radio spectra are shown in the left panel of Figure 3 for several values of the density normalization. These values are chosen so that the model spectra embrace the observed radio flux densities. The red line with a 10 times higher density profile than that shown in Figure 1 gives the best fit to the observed spectrum.

However, the high gas density implies strong X-rays via the bremsstrahlung process from the two torii evident in the density profile of Figure 1. The bremsstrahlung emission coefficient is calculated by (Rybicki & Lightman 1979):

$$\mathcal{E}_\nu = 8.5 \times 10^{-39} n^2 T_e^{-1/2} \exp(-h\nu/k_B T_e), \quad (7)$$

where h is the Planck constant. The right panel of Figure 2 shows the bremsstrahlung emission coefficient at ~ 4.1 keV and the corresponding emission spectra are also indicated in the left panel of Figure 3. The bremsstrahlung emission exceeds the observed upper limit for all the three density normalizations. This simple model therefore cannot produce the observed radio flux level without exceeding the X-ray upper limit.

It is well-known that nonthermal synchrotron emission is more efficient than thermal synchrotron. We next study whether a simple nonthermal model with a single power-law electron distribution can account for the radio flux without violating the X-ray upper limit. The electron distribution is given by

$$N(E) = N_0 E^{-p} \quad \text{for } E > E_0, \quad (8)$$

where E_0 is the low energy cutoff. N_0 and E_0 can be calculated with

$$\int_{E_0}^{\infty} N_0 E^{-p} dE = n, \quad (9)$$

$$\int_{E_0}^{\infty} N_0 E^{-p+1} dE = 3nk_B T_e. \quad (10)$$

The corresponding emission and absorption coefficients are given respectively by (Pacholczyk 1970)

$$\mathcal{E}_\nu = c_5(p) N_0 [B \sin \alpha]^{(p+1)/2} \left(\frac{\nu}{2c_1} \right)^{(p-1)/2}, \quad (11)$$

$$\kappa_\nu = c_6(p) N_0 [B \sin \alpha]^{(p+2)/2} \left(\frac{\nu}{2c_1} \right)^{-(p+4)/2}, \quad (12)$$

where α is the angle between the magnetic field and the line of sight and c_i are defined in Pacholczyk (1970). In our calculations we chose $p = 3$ to avoid significant NIR emission in the quiescent-state. As the p increases, the non-thermal emission model became less efficient and closer to the thermal model. The right panel of Figure 3 show the spectra for several density normalizations, where the synchrotron spectrum is cut off artificially at 10^{15} Hz and the bremsstrahlung spectra is given by the thermal formula of equation (7). Compared with the thermal model, more radio emission is produced for a given density normalization. However, to produce the observed radio flux level, the bremsstrahlung emission still exceeds the observed upper limit.

While the outer torus of the simulation is expected to merge with the inner torus if the simulation is run for a long enough time, the inner torus is already relaxed at the present epoch of the simulation. Therefore a longer run may remove the bremsstrahlung emission from the outer torus, we don't expect the overall bremsstrahlung X-ray flux to decrease by more than a factor of 2. It is therefore challenging to produce the observed radio flux level from Sgr A* without exceeding the X-ray upper limit with this simulation. The high X-ray flux as compared with the radio flux is a direct consequence of the high values of plasma β given by this simulation.

$$\beta = \frac{P_{gas}}{B^2/8\pi}. \quad (13)$$

For this simulation, β is always greater than 100 except in the polar regions, where the GRMHD simulation is not reliable and we have excluded these regions while obtaining the emission spectra. The bremsstrahlung emission is determined by the gas temperature and density. The synchrotron emission also depends on the magnetic field. For high values of β , the magnetic field is weak. It is therefore difficult to produce significant radio emission without making X-rays through the bremsstrahlung. Simulations that are capable of producing lower values of β are needed to overcome this challenge. We also noticed that the radio spectra of both the thermal and non-thermal model are too hard to fit the observed spectrum. Decreasing the value of plasma β alone may not explain the observations.

Errors in the divergence of B are handled differently in the Cosmos++ than the HARM code (Gammie et al. 2003; Anninos et al. 2005). The latter uses a constrained transport schemes for evolving the induction equation whereas Cosmos++ does not. As a consequence, the HARM code appears to be able to produce lower values of plasma β . We ran the HARM code in a domain of $100 r_S$ in radius with the torus pressure maximum initially at $\sim 6 r_S$. The simulated disk structure in a late time when the initial torus has completely relaxed is shown in Figure 4. The simulation produces more than 10 times stronger magnetic fields with comparable values for the density maximum. Figure 5 gives the corresponding emission coefficient maps. Although the synchrotron emission may be comparable to that in Figure 4, we expect much less bremsstrahlung X-rays due to the compactness of the torus in this latter simulation. The left panel of Figure 6 shows the spectra of the thermal model with several density normalizations. The bremsstrahlung X-ray emission is far below the observed upper limit. However, the radio spectra are still not flat enough to fit the observed spectrum.

Higher frequency emission is produced at relatively smaller radii, where the magnetic field is strong and the gas temperature is high. The fact that the model predicted spectrum is harder than the observed spectrum suggests that emission from small radii needs to be suppressed to produce a softer spectrum. The synchrotron cooling time of electrons at smaller radii is shorter. It is possible that the electron temperature is actually lower than the gas temperature at small radii. Modeling of the emission from a small accretion torus also favors a lower electron temperature than the gas temperature (Liu et al. 2007; Noble et al. 2007; Huang et al. 2008). We model the electron temperature with

$$T_e = \left(\frac{r}{R}\right)^\delta T, \quad (14)$$

where R is the radius, beyond which electrons reach thermal equilibrium with the ions and δ is a free parameter determined by the electron heating and cooling processes.

There was no need to apply the two-temperature model to the first simulation because it would decrease the amount of NIR and radio emissions without decreasing the

bremsstrahlung emission values, we would still have the same problem of exceeding the upper limits imposed by *Chandra* on the X-ray emission. We applied this two-temperature model with $R = 10 r_S$ and $\delta = 1.0$ to the second simulation and calculated the thermal emission spectrum. The right panel of Figure 6 shows the results. The model with a 1000 times higher density than that in Figure 4 fits the radio spectrum reasonably well. The underproduction of radio emission below 10 GHz is due to the relatively small simulation domain of $100 r_S$. Most of the longer wavelength emission is produced beyond $100 r_S$. However, the model predicted X-ray flux level just matches the X-ray upper limit. So this model fits the observations marginally. Including the Doppler effect and considering the possibility of nonthermal emission may improve the fitting.

3. Conclusions

Sgr A* is a radio source powered by accretion into a black hole. Modeling the emission from this radio source at the Galactic center provides us with knowledge of the dynamics of the accretion flow near black holes and helps us further understand the plasma physics processes of the accretion torus. We were unsuccessful in our attempt to reproduce the observed spectrum using simulations with very high values of plasma β . With the HARM code, lower values of plasma β are produced. Although we were able to apply a two temperature model to this simulation to correctly match the shape of the observed radio emission spectrum, we had the reoccurring problem of exceeding the upper-bound imposed by *Chandra* in the X-ray emission spectrum. We also note that the HARM simulation has a much smaller initially torus, which effectively reduces the bremsstrahlung X-ray flux. Although this itself may suggest that the angular momentum of the accretion flow must be low (Coker & Melia 1999; Rockefeller et al. 2004), one needs to explore the dependence of the bremsstrahlung X-ray emission on the size of the initial torus to quantify this constraint.

The above challenge of modeling observations of Sgr A* with GRMHD simulations may be alleviated by several means. First, as we have shown in the paper, nonthermal synchrotron emission is more efficient than thermal synchrotron and in the nonthermal scenario the radio spectrum may be fitted with a lower density normalization than the thermal one, which reduces the bremsstrahlung X-ray flux. The Doppler effect, which we didn't consider in the current study, is expected to boost the radio emission as well. Introducing a black hole spin, one can produce even lower values of plasma β and higher Doppler boosting, both of which will enhance the radio emission. Lastly, the bremsstrahlung X-ray may be suppressed by reducing the mean density in the accretion disk through the tilt of the accretion disk with respect to the black hole spin (Liu & Melia 2002b). Three dimensional simulations are then

needed to quantify this effect (Rockefeller et al. 2005; Fragile et al. 2007).

In our modeling, we haven't studied the dependence of the model spectrum on the inclinational angle of the accretion disk, the GR effect, and the transfer of polarized emission. However, the radio spectrum is expected to have very weak dependence on these factors. Nevertheless, they should be included in a more complete study.

4. Acknowledgments

I would like to thank my mentor Siming Liu for guiding me throughout the duration of this project. I would like to also thank Chris Fragile and Cong Yu for running the simulations. I would like to also thank James Colgan and Norm Magee for all of their help during this summer. Thanks to the NSF in part for funding. I would finally like to thank UNM, Los Alamos and Sally Siedel for giving me the opportunity to participate in this great program.

REFERENCES

- Aitken, D. K., et al. 2000, *ApJ*, 534, L173
- An, T., Goss, W. M., Zhao, J. -H., Hong, X. Y., Roy, S., Rao, A. P., & Shen, Z.-Q. 2005, *ApJ*, 634, 49
- Anninos, P., Fragile, P. C., & Salmonson, J. D. 2005, *ApJ*, 635, 723
- Baganoff, F. K., et al. 2001, *Nature*, 413, 45
- Baganoff, F. K., et al. 2003, *ApJ*, 591, 891
- Balbus, S. A., & Hawley, J. F. 1991, *ApJ*, 555, L83
- Bélanger, G., Goldwurm, A., Melia, F., Ferrando, P., Grosso, N., Porquet, D., Warwick, R., & Yusel-Zadeh, F. 2005, *ApJ*, 635, 1095
- Bower, G. C., Wright, M., Falcke, H., & Backer, D. C. 2001, *ApJ*, 555, 103
- Bower, G. C., Falcke, H., Herrnstein, R. M., Zhao, J.-H., Goss, W. M., & Backer, D. C. 2004, *Science*, 304, 704
- Broderick, A. E., & Loeb, A. 2005, *MNRAS*, 363, 353
- Bromley, B., Melia, F., & Liu, S. 2001, *ApJ*, 555, L83
- Coker, R., & Melia, F. 1999, *ApJ*, 511, 750
- De Villiers, J., & Hawley, J. 2003, *ApJ*, 589, 458
- Dodds-Eden et al. 2009, arXiv: 0903.3416
- Eckart, A., et al. 2004, *A&A*, 427, 1
- Eckart, A., et al. 2006, *A&A*, 450, 535
- Falcke, H., & Markoff, S. 2000, *AA*, 362, 113
- Falcke, H., Melia, F., & Agol, E. 2000a, *ApJ*, 528, L13
- Falcke, H., Goss, W. M., Matsuo, H., Teuben, P., Zhao, J.-H., & Zylka, R. 1998, *ApJ*, 499, 731
- Fragile, P. C., Blaes, O. M., Anninos, P., & Salmonson, J. D. 2007, *ApJ*, 668, 417

- Gammie, C. F., McKinney, J. C., & Tóth, G. 2003, *ApJ*, 589, 444
- Genzel, R. et al. 2003, *Nature*, 425, 934
- Ghez, A. M., et al. 2004, *ApJ*, 601, L159
- Ghez, A. M., et al. 2005, *ApJ*, 635, 1087
- Goldston, J. E., Quataert, E., & Igumenshchev, I. V. 2005, *ApJ*, 621, 785
- Hawley, J. F., Beckwith, K., & Krolik, J. H. 2007, *ApSS*, 311, 117
- Herrnstein, R. M., Zhao, J.-H., Bower, G. C., & Goss, W. M. 2004, *ApJ*, 127, 3399
- Huang, L., Liu, S., Shen, Z. Q., Cai, M., Li, H., & Fryer, C. L. 2008, *ApJ*, 676, L119
- Liu, S., & Melia, F. 2001, *ApJ*, 561, L77
- Liu, S., & Melia, F. 2002, *ApJ*, 566, L77
- Liu, S., & Melia, F. 2002b, *ApJ*, 573, L23
- Liu, S., Petrosian, V., Melia, F., & Fryer, C. L. 2006, *ApJ*, 648, 1020
- Liu, S., Qian, L., Wu, X., Fryer, C. L., & Li, H. 2007, *ApJ*, 668, L127
- Mahadevan, R., Narayan, R., & Yi, I. 1996, *ApJ*, 465, 327
- Markoff, S., Falcke, H., Yuan, F., & Biermann, P. L. 2001, 379, L13
- Melia, F. 1992, *ApJ*, 387, L25
- Melia, F., Liu, S., & Coker, R. 2000, *ApJ*, 545, L117
- Melia, F., Liu, S., & Coker, R. 2001, *ApJ*, 553, 146
- Nobel, S. C., Gammie, C. F., McKinney, J. C., & Del Zanna, L. 2006, *ApJ*, 641, 626
- Nobel, S. C., Leung, P. K., Gammie, C. F., & Book, L. G. 2007, *Class. Quantum Grav.*, 24, S259
- Pacholczyk, A. G. 1970, *Radio Astrophysics* (San Francisco: Freeman), 86
- Porquet, D., et al. 2003, *A&A*, 407, L17
- Rockefeller, G., Fryer, C. L., Melia, F., & Warren, M. S. 2004, *ApJ*, 604, 662

- Rockefeller, G., Fryer, C. L., & Melia, F. 2005, *ApJ*, 635, 336
- Rybicki, G. B., & Lightman, A. P. 1979, *Radiative Processes in Astrophysics* (John Wiley & Sons), 160
- Schödel, R., et al. 2002, *Nature*, 419, 694
- Shen, Z.-Q., Lo, K. Y., Liang, M.-C., Ho, T. P., & Zhao, J.-H. 2005, *Nature*, 438, 62
- Tagger, M., & Melia, F. 2006, *ApJ*, 636, L33
- Xu, Y. et al. 2006, *ApJ*, 640, 319
- Yuan, F., Quataert, E., & Narayan, R., 2003, 598, 301
- Yusef-Zadeh, F., et al. 2006, *ApJ*, 644, 198
- Yusef-Zadeh, F., Wardle, M., Cotton, W. D., Heinke, C. O., & Roberts, D. A. 2007, *ApJ*, 668, 47
- Yusef-Zadeh, F., Wardle, M., Heinke, C., Dowell, C. D., Roberts, D., Baganoff, F. K., & Cotton, W. 2008, *ApJ*, 682, 361
- Zhao, J. H., Herrnstein, R. M., Bower, G. C., Goss, W. M., & Liu, S. 2004, *ApJ*, 603, L85

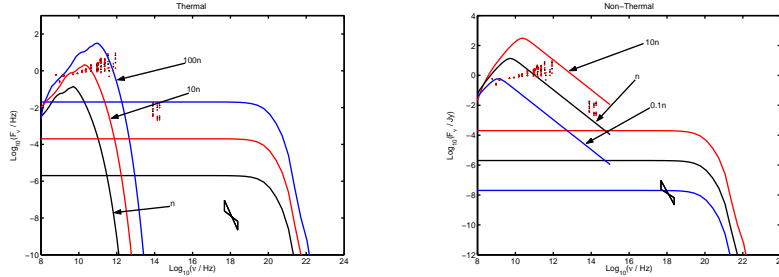


Fig. 3.— *Left*: Thermal synchrotron and bremsstrahlung emission spectra for the one temperature model. The black, red, and blue lines correspond to the particle density in Figure 1, 10, and 100 times this density, respectively. As expected, the bremsstrahlung flux level scales with the density squared. The radio to sub-millimeter data was obtained from observations over the past decade. The scattering of the millimeter and sub-millimeter data is caused by the variability of the source. The NIR flux densities are for flares observed during the past few years and therefore should be considered as upper limit for the “quiescent” state emission from the accretion flow. The butterfly is given by *Chandra* observations of the quiescent state X-ray emission, which appears to be dominated by thermal emission at large radii. Thus it also should be interpreted as an upper limit for X-ray emission from the small scale accretion flow. All the bremsstrahlung spectra exceed this upper limit for X-ray emission. *Right*: Same as the left panel but for the non-thermal model with a single power-law electron distribution with a low energy cutoff. The synchrotron spectra are showed up to 10^{15} Hz. The density normalization is indicated in the figure. Compare with the thermal models in the left panel, the nonthermal model is more efficient in the synchrotron emission process. However, to match the observed radio flux level, the bremsstrahlung X-ray flux still exceeds the observed upper limit.

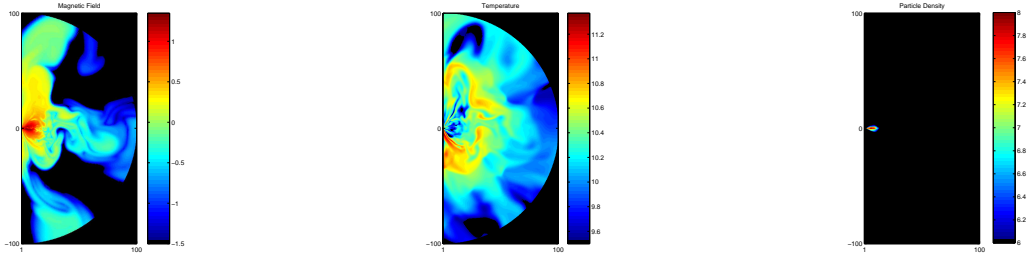


Fig. 4.— Same as Figure 1 but for a simulation with the HARM with a zero black hole spin.

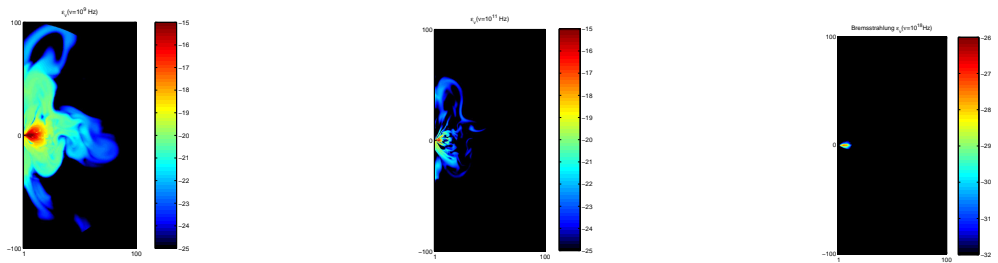


Fig. 5.— Same as Figure 2 but for the simulation of Figure 4.

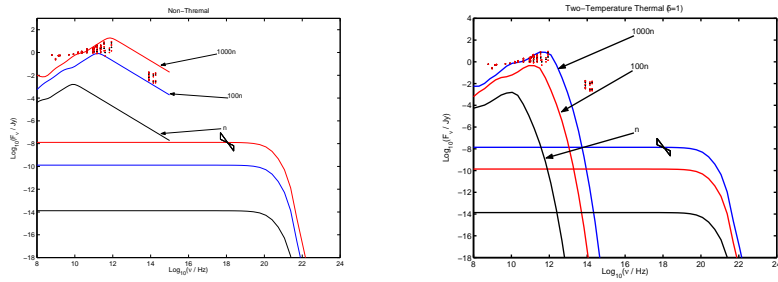


Fig. 6.— *Left*: The same as the left panel of Figure 3 but for the simulation of Figure 4. *Right*: The same as the left panel except that electron temperature is lower than the gas temperature toward small radii as given by equation (14) with $R = 10 r_S$ and $\delta = 1.0$.